Improved Stability of $FAPbI_3$-Based Mixed-Cation Perovskite Solar Cells Fabricated Using Facile Cation Injection Technology

Soo Beom Hong and Hyung Wook Choi

***Abstract*—Compositional engineering adding organic and inorganic cations is considered one of the effective ways to improve the optoelectronic performance of PSCs. However, investigations of mixed-cations in PSCs are still a nascent area of research. In this study, an anti-solvent suitable for the preparation of mixed-cation perovskite was first adopted. We presented a simple surface engineering technique for manufacturing mixed-cation perovskite by injecting cations through the process of post-treatment of the adopted anti-solvent treated pure $FAPbI_3$ film with methylammonium iodide (MAI) solution. The prepared mixed-cation perovskite film showed uniform particle size, particle growth, and significantly improved short-circuit current, charge coefficient, device efficiency and device stability.**

***Index Terms*—Photovoltaic cells, thin films, optoelectronic and photonic sensors.**

I. Introduction

LEAD halide perovskite was first reported in 2009 as a photosensitizer for dye-sensitized solar cell structures and began to attract the attention of researchers [1]. Perovskite has advantages that include high power conversion efficiency (PCE), low cost, long carrier diffusion length, tunable bandgap, and very low exciton binding energy [2]. Currently, lead halide perovskite is one of the most promising candidates to replace the crystalline silicon-based solar cells that have dominated the huge photovoltaic market [3]. An organic-inorganic metal halide perovskite material has an ABX_3 structure, where A is a monovalent organic cation [($CH_3NH_3^+$ (MA^+) or $CH_3(NH_2)_2^+$ (FA^+)]) or inorganic cation (Cs^+ or Rb^+), B is a divalent metal cation (Pb^{2+} or Sn^{2+}), and X^- is a halide anion (Cl^-, Br^-, I^-) [4]. By tuning the material composition of ABX_3, we can determine the optoelectronic properties of perovskites. Adjusting the material composition of A can increase the chemical stability [5], and altering the composition of B can change the light absorption spectrum, energy level, and transport properties [6]. In addition, changing the composition of X provides the option of adjusting the bandgap [7]. $FAPbI_3$ has recently been highlighted as a material for perovskite solar cells (PSCs), and this material has a narrow band gap of approximately 1.43–1.50 eV and excellent light absorption [8]. However, preparing efficient, stable high-quality $FAPbI_3$ films is difficult because of its unstable phase stability. The α-phase of $FAPbI_3$ is easily transformed into a "yellow" δ-phase $FAPbI_3$. This transformation results in limited film stability and photovoltaic performance [9], [10]. Another factor that changes the photovoltaic performance of the film is the amount of PbI_2. Excessive PbI_2 delays electron transport, lowers the efficiency owing to the reduced charge rate and low short-circuit current density (J_{SC}), and promotes the degradation of PSCs under continuous illumination, a factor that negatively affects device performance [11]. However, in the case of PSCs with an appropriate amount of PbI_2, defects in the perovskite film can be protected to the benefit of the efficiency of PSCs and can help with low charge carrier mobility and reduced electron injection into titanium dioxide (TiO_2) [12], [13]. Therefore, optimizing the amount of PbI_2 plays an important role in PSC fabrication. One way to increase the phase stability of perovskites is to add anions or cations to the perovskite chemical structure [14]. Small amounts of MA^+ induce high crystallization in FA-based perovskite films, resulting in a more structurally stable composition than $FAPbI_3$. In addition, the finished mixed-cation perovskite film has a low hysteresis coefficient and improved device performance [15], [16]. However, $FA_xMA_{1-x}PbI_3$ mixed-cation perovskite leads to shape-related phase separation, low crystallinity, and poor film morphology and crystal structure. Therefore, a new method for manufacturing mixed-cation perovskites is needed.

The anti-solvent process is one of the most widely used methods for producing high-quality perovskite films by improving the crystallization of the film and uniformity of the surface [17]. The typical anti-solvents used by researchers to increase device efficiency are chlorobenzene (CB), toluene (TL), and diethyl ether (DE) [18]. A method of reacting the finished perovskite film once more using a mixture of cations or anions is called a post-treatment method. Post-treatment improves the optoelectronic properties of the film by promoting crystallite regrowth and improving the surface morphology and structure of the film to produce a high-quality film. In addition, the amount of unreacted PbI_2 remaining is controlled by reacting the unreacted PbI_2 [19].

In this study, a mixed-cation perovskite thin film was prepared by surface treatment of the film using the methylammonium iodide (MAI) post-treatment method. The prepared film had

Manuscript received January 19, 2022; revised April 1, 2022; accepted April 13, 2022. Date of publication April 22, 2022; date of current version May 4, 2022. This work was supported in part by the Basic Science Research Capacity Enhancement Project through the Korea Basic Science Institute (National Research Facilities and Equipment Center) and funded by the Ministry of Education under Grant 2019R1A6C1010016 and in part by the Gachon University Research Fund of 2020 under Grant GCU-2020084500 09. *(Corresponding author: Hyung Wook Choi.)*

The authors are with the Electrical Engineering Department, Gachon University, Seongnam-Si 13120, Korea (e-mail: cldkrml@gachon.ac.kr; chw@gachon.ac.kr).

Digital Object Identifier 10.1109/JPHOT.2022.3168064

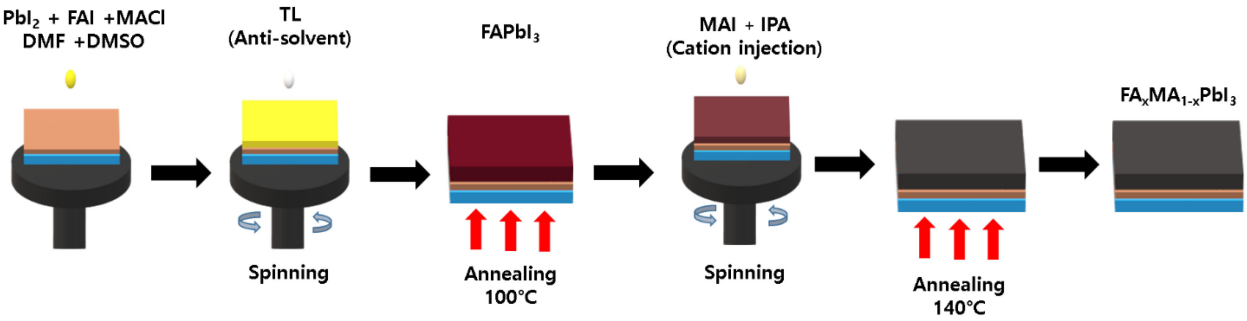

Fig. 1. Schematic illustration of the fabrication process for obtaining a high-quality particle morphology and high crystallinity perovskite using the methylammonium iodide (MAI) post-treatment method.

improved phase stability and reduced surface defects; therefore, the absorbance due to grain growth also increased. In addition, by studying the amount of MAI added to the film, the effect of the added MAI on the film was analyzed, and an optimized film was successfully produced. In summary, we improved the solar performance bysuppressing particle size growth and surface defects through an anti-solvent process using TL and MAI post-treatment. This process also contributed to the efficiency improvement by passivating the perovskite and leaving an appropriate amount of PbI_2. The optimized mixed-cation perovskite solar cell increased the fill factor (FF), open-circuit voltage (V_{OC}), and Jsc. In addition, the efficiency increased by 2.37% on average.

II. Experimental Setup

A. Reagents and Materials

Fluorine-doped tin oxide (FTO) glass (7 Ω sq^{-1}) was purchased from Wooyang GMS (Pyeongtaek, South Korea). Titanium diisopropoxide bis(acetyl-acetonate), 1-butyl alcohol (99%), ethyl alcohol ($\geq$99.5%), acetonitrile (99.93%), lead iodide (PbI_2, 99.999%), N,N-dimethylformamide (DMF, 99.8%), dimethyl sulfoxide (DMSO, $\geq$99.9%), 2-propanol (IPA; 75 wt%), 22,77-tetrakis[N,N-di(4-methoxypheny l)amino]-99-spirobifluorene (spiro-OMeTAD, 99%), bis(tri fluoromethane)sulfonimide lithium salt (Li-TSFI; $\geq$ 99.0%), chlorobenzene (99.8%), toluene (99.9%), diethyl ethyl ($\geq$99.7%), and 4-tertbutylpyridine (98%) were purchased from Sigma-Aldrich (St. Louis, MO, USA). Formamidinium iodide (FAI), methylammonium iodide (MAI), methylam monium hydrochloride (MACl), and titanium nanoparticle paste (18NR-T) were purchased from GreatCell Solar (Queanbeyan, Australia). All reagents were used as received without further purification.

B. Device Preparation

FTO-coated glass was ultrasonically washed with acetone, ethanol, and distilled water to remove impurities. FTO was used as the substrate for the device fabrication. The FTO was exposed to ultraviolet (UV) ozone for 20 min. The TiO_2 compact layer solution (55 μL of Titanium diisopropoxide bis(acetyl-acetonate) in 1 mL 1-butanol) was spin-coated on FTO-coated glass at 3000 rpm for 20 s and annealed at 125 °C for 12 min. The mesoporous TiO_2 layer was spin-coated at 3000 rpm for 20 s using a TiO_2 paste solution (18NR-T / ethanol 1:6 v/v), followed by annealing at 480 °C for 60 min. The perovskite $FAPbI_3$ precursor solution was prepared by mixing lead iodide (1.4 mol) and formamidinium iodide (1.4 mol) in an DMSO: DMF (10:1 v/v) solvent system. MACl was added to the prepared precursor solution and stirred for 30 min. The solution was spin-coated onto mesoporous TiO_2 at 4500 rpm for 20 s. 10 s before the end of spin coating, 200 μL of CB, TL or DE was slowly dropped onto the center of the spinning film. The prepared film was annealed at 80 °C for 5 min and at 100 °C for 10 min. For MAI post-treatment, IPA and MAI (5, 10, 15, 20 mg) were stirred for 1 h. The post-treatment solution (50 µL) was dropped onto the surface of the prepared $FAPbI_3$ surface for 5 s and rotated at 4500 rpm for 20 s. The MAI post-treated films were then annealed at 100 °C for 5 min and 140 °C for 10 min.

C. Device Characterization

An Agilent 8453 UV-visible (UV-vis) spectrophotometer (Agilent 8453, Agilent Technologies, Santa Clara, CA, USA) was used to measure the UV-vis absorption spectra. The phases of the perovskite films were analyzed using Cu Kα radiation (λ = 0.1542 nm) with a Rigaku DMAX 2200 X-ray diffraction (XRD) system (Rigaku, Tokyo, Japan). Cross-sectional and surface data of the perovskite layer were obtained using scanning electron microscopy (SEM, Hitachi S-4700, Tokyo, Japan). The J-V curve data of the PSC was obtained using a solar simulator (Polaromix K201, Solar simulator LAB 50, McScience K3000, McScience, Suwon, Korea) at 1 illuminance of sunlight (AM1.5G, 100 mW cm^{-2}).

III. Results And Discussion

Fig. 1 shows the step-by-step process for preparing mixed-cation perovskite films using the MAI post-treatment method. First, a perovskite precursor solution containing MACl, FAI, and PbI_2 in a DMF and DMSO solvent mixture was spin-coated on an FTO substrate, underwent an anti-solvent process using TL, and then was annealed to form a $FAPbI_3$ film. Then, MAI post-treatment was performed. The solution for MAI post-treatment was prepared by dissolving MAI (0, 5, 10, 15, and 20 mg) in 1000 mL IPA. For the convenience of discussing the results, the manufactured films are denoted as MAI-0, MAI-5, MAI-10, MAI-15, and MAI-20.

The various solvents used in the anti-solvent process affect the perovskite films in the early stages of crystallization [20]. Therefore, proper solvent selection plays an important role in

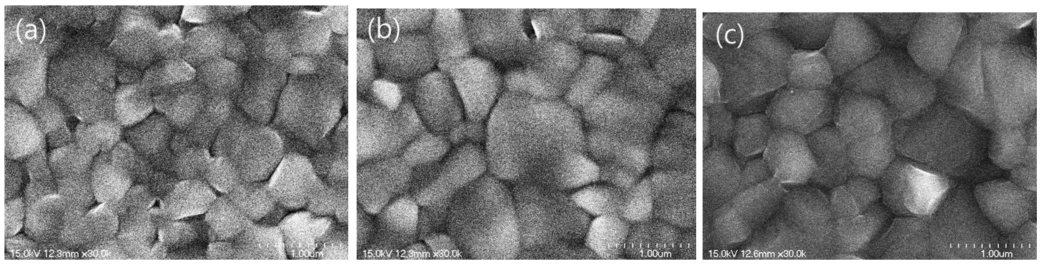

Fig. 2. Scanning electron microscopy (SEM) images of films with different anti-solvent solvents. (a) Diethyl ether (DE), (b) chlorobenzene (CB), and (c) toluene (TL).

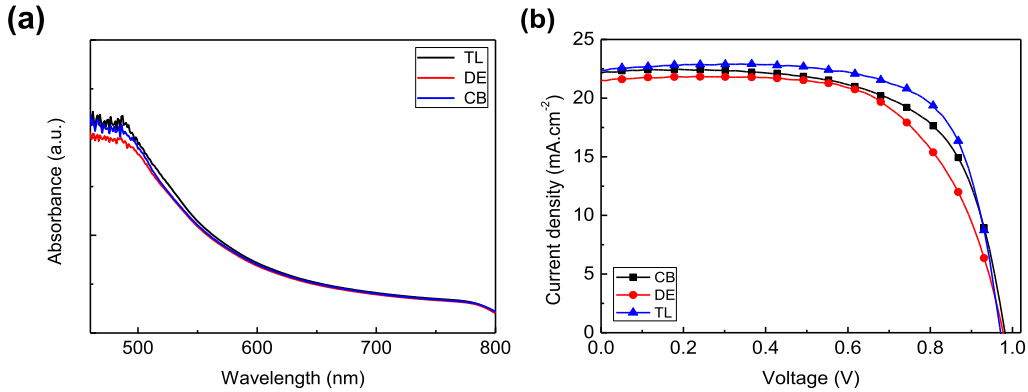

Fig. 3. (a) Ultraviolet-visible (UV-vis) absorption spectra of perovskite films treated with different anti-solvents toluene (TL), diethyl ether (DE), and chlorobenzene (CB). (b) J-V curves.

producing high-quality perovskite films. The surface morphology and uniformity of the films were investigated using SEM. Fig. 2 shows SEM images of perovskite thin films prepared using DE, CB, and TL as anti-solvent solvents. The DE-treated films had small grain sizes and pinholes, whereas the CB-and TL-treated films had relatively large grain sizes and almost no visible pinholes. The average particle diameters of the perovskite films treated with DE, CB, and TL were approximately 570 nm, 614 nm, and 641 nm, respectively. The particle size was larger than that of the film. These results indicated that the type of anti-solvent affected the perovskite surface and crystallinity. Therefore, among the anti-solvents, TL was the most useful for improving surface area coverage and increasing particle area.

Fig. 3(a) shows the results of UV-vis spectroscopy measurements to evaluate the light absorption capacity of the films prepared using various anti-solvents. The UV-vis absorption spectra cover a wide range of wavelengths from the visible to the near-infrared region. The UV-vis absorbance performance of the films decreased in the order of TL, CB, and DE. The absorption spectrum of the CB-treated film was broader than that of the DE-treated film because of the chemical reaction between the precursor solvents [21]. In addition, the TL-treated film induced the perovskite precursor into a metastable region rather than a supersaturated region, thereby exhibiting excellent light absorption; thus, the TL-treated film exhibited the highest light absorption coefficient [22].

Fig. 3(b) shows the current density-voltage (J-V) curves for three different cells treated with different anti-solvent solvents. Further details on the photovoltaic properties are presented in Table I. The PCEs for films treated with DE, CB, and TL were

TABLE I
PARAMETERS AT THE HIGHEST PERFORMANCE OF THE DEVICE ACCORDING TO THE TYPE OF ANTI-SOLVENT

	DE	CB	TL
J_{SC} (mA cm^{-2})	21.51	22.15	22.31
V_{OC} (V)	0.97	0.98	0.98
FF (%)	63.89	65.98	72.44
PCE (%)	13.45	14.34	15.94

13.45%, 14.34%, and 15.94%, respectively. Films treated with TL had the highest efficiency with the highest J_{SC} and FF. This result may be due to better uniformity of the perovskite film and less sharp grain boundaries. These results were representative of the effect of anti-solvents on PCE. Therefore, subsequent mixed-cation perovskite films should use TL as the most suitable anti-solvent.

The surface morphology and uniformity of the films were confirmed using SEM. Fig. 4 shows SEM images of perovskite thin films subjected to post-treatment with various concentrations of MAI solutions. In Fig. 4(a), the surface of MAI-0 had small crystals and a particle distribution that indicated non-uniform growth, and the particle size of the perovskite film increased as the amount of MAI increased. For a detailed analysis of the MAI post-treated films, the particle distribution was investigated by calculating the average particle size. The calculations confirmed

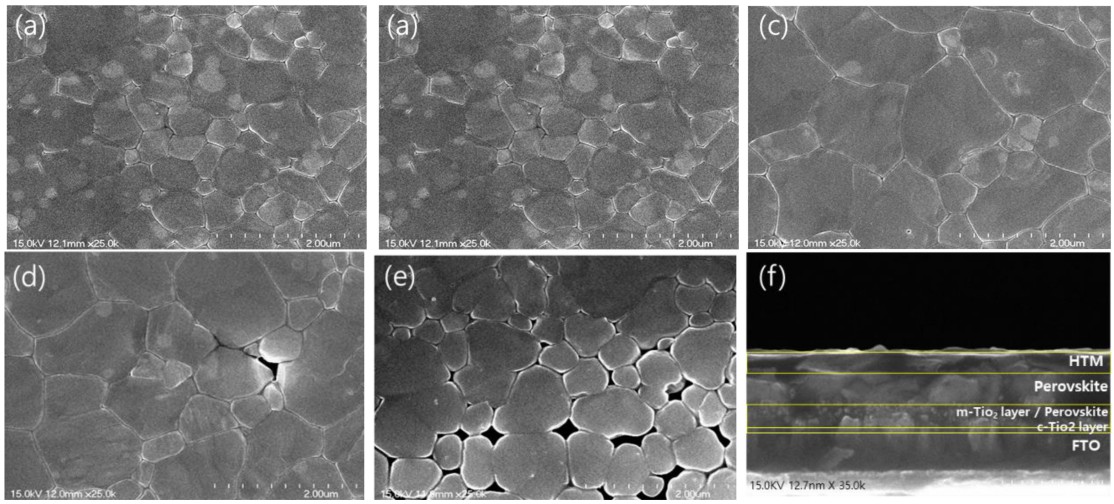

Fig. 4. Scanning microscopy (SEM) images of films post-treated with methylammonium iodide (MAI)at various concentrations (mg mL-1). (a) MAI-0, (b) MAI-5, (c) MAI-10, (d) MAI-15, (e) MAI-20, and (f) cross-sectional SEM image of a post-treated film.

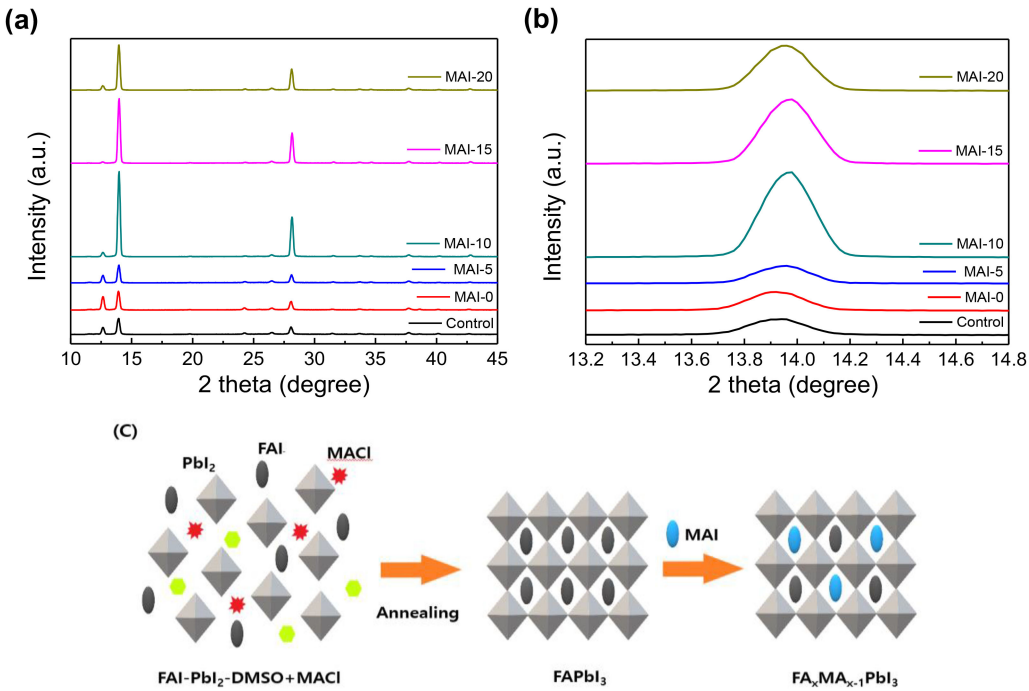

Fig. 5. (a) X-ray diffraction (XRD) pattern according to the concentration of the film post-treated with methylammonium iodide (MAI). (b) Extended XRD region around 13.9°. (c) Formation process of mixed-cation $FA_XMAI_{1-X}PbI_3$ perovskite prepared using MAI post-treatment.

that the average particle size was approximately 562 nm for MAI-0, 703 nm for MAI-5, 860 nm for MAI-10, 1240 nm for MAI-15, and 1560 nm for MAI-20. Films prepared using MAI-10 had larger particles and less coverage compared to those prepared using other concentrations of MAI. However, as the amount of MAI added increased to 15 mg mL^{-1}, the size and number of pinholes also increased. This increase in particle size implied improved optoelectronic parameters. The increase in the size of the pinholes was due to the shrinkage of the perovskite particles and structural stress caused by the high MAI concentration. [23]. As a result, the main cause of the morphological deformation of the perovskite surface was the MAI concentration. Therefore, the MAI post-treatment method strongly affected the crystallinity and surface morphology of the $FAPbI_3$ films. In short, the film treated with an appropriate amount of MAI improved the photoelectric performance by increasing the light absorption owing to the improved particle size and dense particle distribution

The crystallinity and phase characteristics determined by XRD of the perovskite film prepared using the MAI post-treatment method are shown in Fig. 5(a). The diffraction peaks at 13.9° and 27.8° corresponded to the (001) and (002) planes of $FAPbI_3$ perovskite, respectively. There were no significant changes in the XRD patterns of MAI-0 and 5, even though the MAI post-treatment method was applied to the latter sample. When the amount of MAI was increased to 10 mg, the intensity

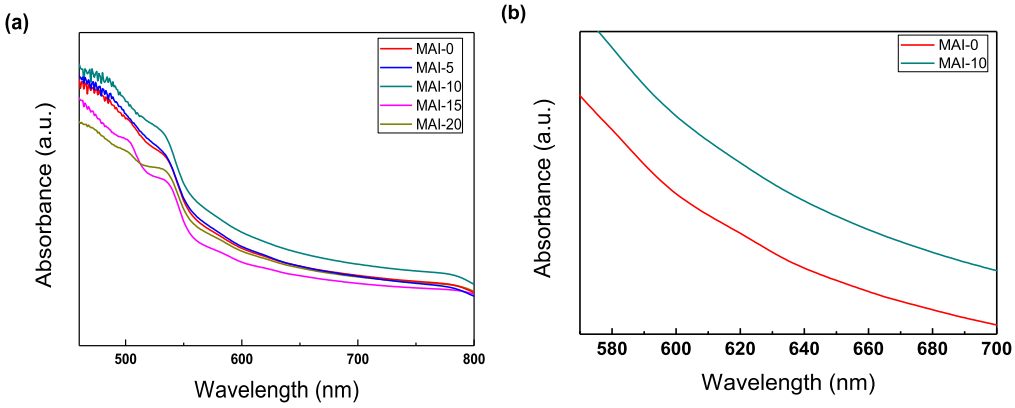

Fig. 6. (a) Ultraviolet-visible (UV-vis) absorption spectra of the mixed-cation perovskite film $FA_xMA_{x-1}PbI_3$ treated with different concentrations of methylammonium iodide (MAI). (b) Magnified fingerprint area of UV-vis absorption spectra for the MAI-0 and MAI-10 film.

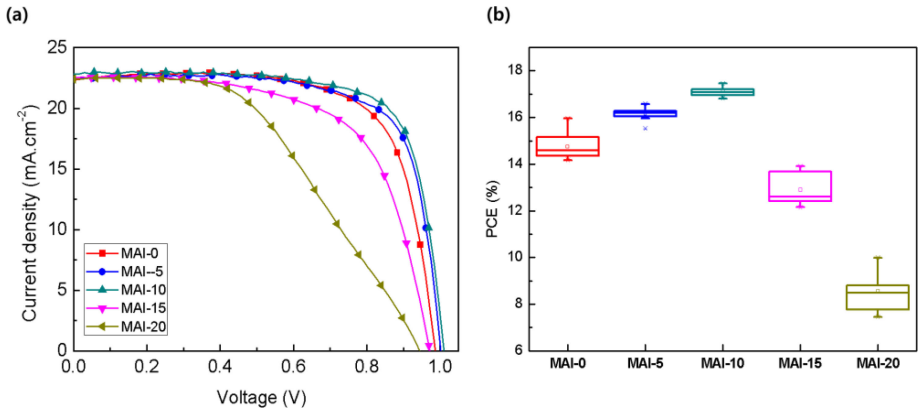

Fig. 7. Performance of solar cells post-treated with various concentrations of methylammonium iodide (MAI) (a) Best J-V curve of the device, (b) Average of 10 power conversion efficiencies (PCEs) of the device.

of the perovskite peak increased sharply, indicating that the crystallinity of the perovskite film was greatly improved. However, the peak intensities of MAI-15 and 20 decreased slowly. This decrease in peak intensity is because the annealing temperature and time affect the film formation as the amount of MA^+ cations injected into the

$FAPbI_3$ film increases. [24] In the case of $MAPbI_3$ film, it starts to decompose slowly when the annealing temperature rises above 120 degrees. Therefore, the peak intensity decreases and PbI_2 also begins to appear in MAI-20. These results were consistent with the results of the previously investigated particle morphology changes. In Fig. 5(b), as the MAI concentration increased, the $FAPbI_3$ main peak moved from 13.9° to 14.2° to coincide with the $MAPbI_3$ main peak. This peak shift proved that the $FA_XMAI_{1-X}PbI_3$ film was formed.

In Fig. 5(a), the peak near 12.6° was the peak for unreacted PbI_2. Films treated with the post-treatment solution without MAI had higher PbI_2 peaks compared to the control film without post-treatment. However, after the addition of MAI, the PbI_2 peak decreased and then increased again in MAI-20. These results indicated that PbI_2 was detected because excessive amounts of MAI adversely affected perovskite formation. In summary, the surface morphology, microstructure, and optoelectronic properties of the film were improved by adding an appropriate amount of PbI_2 using the MAI post-treatment method [13], [19]. The schematic reaction mechanism of the MAI post-treatment method is presented in Fig. 3(c) [25].

As shown in Fig. 6(a), the absorbance was improved in the entire wavelength range as the amount of MAI increased in the UV-vis absorption spectra. However, after MAI-10, the extinction coefficient and absorbance both decreased. This decreased absorbance was caused by the increased pinhole size and crystal shrinkage due to the excessive amount of MAI. [26] The spectra of MAI-0 and MAI-10 were compared in detail by magnifying the fingerprint region of UV-vis absorbance in Fig. 6(b), and this magnified region confirmed the improved photoelectric performance of the MAI post-treatment film. As shown in the above SEM and XRD results, these results were influenced by the grain size increase, surface uniformity, and grain growth of the perovskite film.

Fig. 7(a) shows the solar performance with the J-V curve of PSCs measured by the solar simulator. Fig. 7(b) shows the average PCE of the device. The performance parameters for the post-treatment results with various concentrations of MAI are summarized in Tables II and III. The Jsc of the highest performing device (MAI-10) was 23.40 (mA cm^{-2}), and this value was an improvement compared to the value (22.74 mA cm^{-2}) of the device without MAI treatment (MAI-0). This result was confirmed by the strong light absorption and was consistent with the result of the UV-vis absorbance graph presented above that was closely related to surface defects and trapping. The

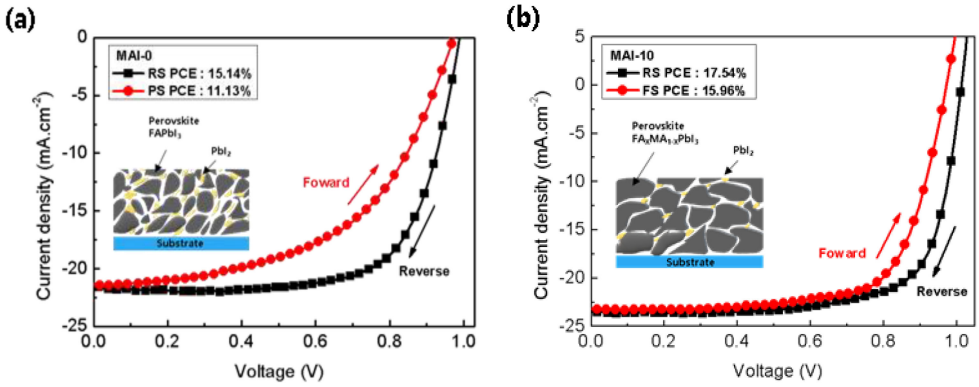

Fig. 8. Forward and reverse dependent J-V characteristics observed for FTO/Tio_2/Perovskite/HTM/Au PSCs (a) MAI-0, (b) MAI-10.

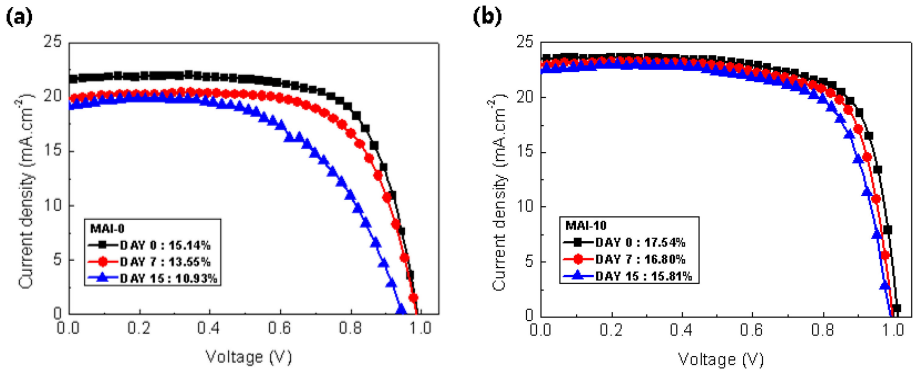

Fig. 9. Stability comparison of mixed-cation PSCs prepared by post-treatment with MAI (a) MAI-0, (b) MAI-10.

TABLE II
PARAMETERS AT PEAK PERFORMANCE OF THE POST-TREATMENT UNIT ACCORDING TO THE AMOUNT OF METHYLAMMONIUM IODIDE (MAI)

Best	MAI-0	MAI-5	MAI-10	MAI-15	MAI-20
J_{SC} (mA cm^{-2})	22.32	22.41	22.84	22.57	22.21
V_{OC} (V)	0.98	1.00	1.00	0.97	0.95
FF (%)	72.45	73.85	74.70	63.44	46.57
PCE (%)	15.94	16.58	17.24	13.91	9.79

TABLE III
AVERAGE PARAMETERS OF THE POST-TREATMENT UNIT ACCORDING TO THE AMOUNT OF METHYLAMMONIUM IODIDE (MAI)

Average	MAI-0	MAI-5	MAI-10	MAI-15	MAI-20
J_{SC} (mA cm^{-2})	22.74	22.34	23.40	22.05	21.01
V_{OC} (V)	0.91	0.99	1.00	0.94	0.91
FF (%)	71.31	73.06	73.12	61.72	44.40
PCE (%)	14.74	16.18	17.11	12.89	8.52

V_{OC} data in Table III increased from 0.91 V for MAI-0 to 1.00 V for MAI-10. This result proved that the surface shape was improved by the MAI post-treatment process. The FF value increased from 72.45% to 74.7% as the concentration of MAI increased from MAI-0 to MAI-10. The PCE values of MAI-0, MAI-5, MAI-10, MAI-15, and MAI-20 were 15.94%, 16.58%, 17.24%, 13.91%, and 9.79%, respectively. These results were consistent with the results mentioned earlier for the values that determine efficiency. The accuracy of the experimental results was verified using the average PCE of the device. As a result, the MAI post-treatment method improved the surface morphology and increased the particle size, resulting in better optoelectronic performance.

The hysteresis curve is closely related to ion movement. This means that changes in the components of perovskite have a large effect on the hysteresis curve. [27], [28] Also, since hysteresis is related to power conversion efficiency and stability, reducing hysteresis is one way to increase efficiency and stability. [29] Fig. 8. shows the hysteresis curves obtained from the forward scan (FS) and reverse scan (RS) of films prepared with and without the MAI post-treatment process. In the case of MAI-0, the J-V curve appears to decrease sharply when compared to MAI-10. Hysteresis index (defined as HI $= (PCE_{rev} - PCE_{fw})/PCE_{rev}$.) Also, MAI-0 is 0.26 and MAI-10 is 0.09, which is about 3 times difference. [30] These results suggest that the preparation of mixed-cation perovskite by injecting cations through the MAI post-treatment process had an effect on the improvement of the stability of PSC.

One of the important research challenges of PSC is the stability of the device. To study the effect of MAI post-treatment on device stability, the time-dependent changes were recorded at regular intervals and presented in Fig. 9. All devices were stored in an air glove box at room temperature (26 °C) and a relative humidity of ∼40%, and PCE performance measurements were taken at room temperature (24 °C), in air. As a result, devices manufactured through post-treatment with MAI-10 show better

stability than MAI-0. Additionally, the PCE of the devices post-treated with MAI-10 remained ∼90% even after 15 days.

IV. Conclusion

In summary, we present a novel approach for producing mixed-cation perovskite films while controlling the amount of unreacted PbI_2 by efficiently treating the surface of the film using the MAI post-treatment method. After the anti-solvent process with TL, 10 mg mL^{-1} of MAI was dissolved in IPA solution on the prepared $FAPbI_3$ film, and then the post-treatment process was performed. The reaction of unreacted PbI_2 and a mixture of cations and anions in a more suitable material composition was mixed to produce a mixed-cation perovskite film. The $FAPbI_3$ film had non-unform small particles before MAI post-treatment, whereas the film had large particles and high crystallinity after MAI post-treatment. In addition, the hysteresis index was more than three times that of the untreated film, and the PCE of the device was maintained at ∼90% even after 15 days. As a result, the device fabricated by the MAI post-treatment method showed improved optoelectronic properties and high efficiency and excellent stability.

References

[1] N. G. Park, "Perovskite solar cells: An emerging photovoltaic technology," *Mater. Today*, vol. 18, no. 2, pp. 65–72, 2015.

[2] D. Li *et al.*, "Recent progress on stability issues of organic–inorganic hybrid lead perovskite-based solar cells," *RSC Adv.*, vol. 6, no. 92, pp. 89356–89366, 2016.

[3] A. K. Jena, A. Kulkarni, and T. Miyasaka, "Halide perovskite photovoltaics: Background, status, and future prospects," *Chem. Rev.*, vol. 119, no. 5, pp. 3036–3103, 2019.

[4] P. Gao, M. Grätzel, and M. K. Nazeeruddin, "Organohalide lead perovskites for photovoltaic applications," *Energy Environ. Sci.*, vol. 7, no. 8, pp. 2448–2463, 2014.

[5] U.-G. Jong *et al.*, "A first-principles study on the chemical stability of inorganic perovskite solid solutions Cs_{1-x} Rb_x PbI_3 at finite temperature and pressure," *J. Mater. Chem. A*, vol. 6, no. 37, pp. 17994–18002, 2018.

[6] E. Mosconi, P. Umari, and F. D. Angelis, "Electronic and optical properties of mixed Sn–Pb organohalide perovskites: A first principles investigation," *J. Mater. Chem. A*, vol. 3, no. 17, pp. 9208–9215, 2015.

[7] Y. Ye *et al.*, "Nature of the band gap of halide perovskites ABX3 (A = CH3NH3, Cs; B = Sn, Pb; x = Cl, Br, I): First-principles calculations," *Chin. Phys. B*, vol. 24. no. 11, 2015, Art. no. 116302.

[8] S. Pang *et al.*, "NH_2CH NH_2PbI_3: An alternative organolead iodide perovskite sensitizer for mesoscopic solar cells," *Chem. Mater.*, vol. 26, no. 3, pp. 1485–1491, 2014.

[9] F. Cordero *et al.*, "Stability of cubic $FAPbI_3$ from X-ray diffraction, anelastic, and dielectric measurements," *J. Phys. Chem. Lett.*, vol. 10, no. 10, pp. 2463–2469, 2019.

[10] Z. Qiu *et al.*, "Recent advances in improving phase stability of perovskite solar cells," *Small Methods*, vol. 4, no. 5, 2020, Art. no. 1900877.

[11] T. Zhang *et al.*, "A controllable fabrication of grain boundary Pbi_2 nanoplates passivated lead halide perovskites for high performance solar cells," *Nano Energy*, vol. 26, pp. 50–56, 2016.

[12] V. Kapoor *et al.*, "Effect of excess Pbi_2 in fully printable Carbon-based perovskite solar cells," *Energy Technol.*, vol. 5, no. 10, pp. 1880–1886, 2017.

[13] T. J. Jacobsson *et al.*, "Unreacted Pbi_2 as a double-edged sword for enhancing the performance of perovskite solar cells," *J. Amer. Chem. Soc.*, vol. 138, no. 32, pp. 10331–10343, 2016.

[14] W. Rehman *et al.*, "Photovoltaic mixed-cation lead mixed-halide perovskites: Links between crystallinity, photo-stability and electronic properties," *Energy Environ. Sci.*, vol. 10, no. 1, pp. 361–369, 2017.

[15] F. Ji *et al.*, "A balanced cation exchange reaction toward highly uniform and pure phase FA_{1-x} MA_x PbI_3 perovskite films," *J. Mater. Chem. A*, vol. 4, no. 37, pp. 14437–14443, 2016.

[16] Y. Zhang *et al.*, "Optimization of stable quasi-cubic FA_x MA_{1-x} Pbi_3 perovskite structure for solar cells with efficiency beyond 20%," *ACS Energy Lett.*, vol. 2, no. 4, pp. 802–806, 2017.

[17] A. D. Taylor *et al.*, "A general approach to high-efficiency perovskite solar cells by any antisolvent," *Nature Commun.*, vol. 12, no. 1, pp. 1–11, 2021.

[18] S. dPaek *et al.*, "From nano-to micrometer scale: The role of antisolvent treatment on high performance perovskite solar cells," *Chem. Mater.*, vol. 29, no. 8, pp. 3490–3498, 2017.

[19] Y. Jiang *et al.*, "A feasible and effective post-treatment method for high-quality $CH_3NH_3PbI_3$ films and high-efficiency perovskite solar cells," *Crystals*, vol. 8, no. 1, 2018, Art. no. 44.

[20] A. Dubey *et al.*, "A strategic review on processing routes towards highly efficient perovskite solar cells," *J. Mater. Chem. A*, vol. 6, no. 6, pp. 2406–2431, 2018.

[21] L. Yang *et al.*, "Novel insight into the role of chlorobenzene antisolvent engineering for highly efficient perovskite solar cells: Gradient diluted chlorine doping," *ACS Appl. Mater. Interfaces*, vol. 11, no. 1, pp. 792–801, 2018.

[22] X. Zhang *et al.*, "Antisolvent-derived intermediate phases for low-temperature flexible perovskite solar cells," *ACS Appl. Energy Mater.*, vol. 1, no. 11, pp. 6477–6486, 2018.

[23] D. Angmo *et al.*, "Controlling homogenous spherulitic crystallization for high-efficiency planar perovskite solar cells fabricated under ambient high-humidity conditions," *Small*, vol. 15, no. 49, 2019, Art. no. 1904422.

[24] L. C. Chen, C. C. Chen, J. C. Chen, and C. G. Wu, "Annealing effects on high-performance $CH_3NH_3PbI_3$ perovskite solar cells prepared by solution-process," *Sol. Energy*, vol. 122, pp. 1047–1051, 2015.

[25] Y. Yang *et al.*, "Bi-functional additive engineering for high-performance perovskite solar cells with reduced trap density," *J. Mater. Chem. A*, vol. 7, no. 11, pp. 6450–6458, 2019.

[26] X. Zhang *et al.*, "High-efficiency perovskite solar cells prepared by using a sandwich structure MAI–PbI_2–MAI precursor film," *Nanoscale*, vol. 9, no. 14, pp. 4691–4699, 2017.

[27] B. Chen, M. Yang, S. Priya, and K. Zhu, "Origin of J–V hysteresis in perovskite solar cells," *J. Phys. Chem. Lett.*, vol. 7, no. 5, pp. 905–917, 2016.

[28] I. M. Dharmadasa, Y. Rahaq, and A. E. Alam, "Perovskite solar cells: Short lifetime and hysteresis behaviour of current–voltage characteristics," *J. Mater. Sci.: Mater. Electron.*, vol. 30, no. 14, pp. 12851–12859, 2019.

[29] Y. Yang, J. Luo, A. Wei, J. Liu, Y. Zhao, and Z. Xiao, "Study of perovskite solar cells based on mixed-organic-cation FA_{1-x} MA_{1-x} PbI_3 absorption layer," *Phys. Chem. Chem. Phys.*, vol. 21, no. 22, pp. 11822–11828, 2019.

[30] D. Yao, "Hindered formation of photoinactive δ-$FAPbI_3$ phase and hysteresis-free mixed-cation planar heterojunction perovskite solar cells with enhanced efficiency via potassium incorporation," *J. Phys. Chem. Lett.*, vol. 9, no. 8, pp. 2113–2120, 2018.